

## Receptor- and Ligand-Based Study on Novel 2,2'-Bithienyl Derivatives as Non-Peptidic AANAT Inhibitors

Alban Lepailleur,<sup>\*,†</sup> Stéphane Lemaître,<sup>†</sup> Xiao Feng,<sup>†</sup> Jana Sopkova-de Oliveira Santos,<sup>†</sup> Philippe Delagrance,<sup>‡</sup> Jean Boutin,<sup>‡</sup> Pierre Renard,<sup>‡</sup> Ronan Bureau,<sup>†</sup> and Sylvain Rault<sup>†</sup>

Centre d'Etudes et de Recherche sur le Médicament de Normandie, UPRES EA 4258, INC3M FR CNRS 3038, Université de Caen–Basse Normandie, UFR des Sciences Pharmaceutiques, Boulevard Becquerel, 14032 Caen Cedex, France, and Laboratoires Servier, 125, Chemin de Ronde, 78290 Croissy-sur-Seine, France

Received December 13, 2009

Arylalkylamine *N*-acetyl transferase (serotonin *N*-acetyl transferase, AANAT) is a critical enzyme in the light-mediated regulation of melatonin production and circadian rhythm. With the objective of discovering new chemical entities with inhibitory potencies against AANAT, a medium-throughput screening campaign was performed on a chemolibrary. We found a class of molecules based on a 2,2'-bithienyl scaffold, and compound **1** emerged as a first *hit*. Herein, we describe our progress from *hit* discovery and to optimization of this new class of compounds. To complete the study, computational approaches were carried out: a docking study which provided insights into the plausible binding modes of these new AANAT inhibitors and a three-dimensional quantitative structure–activity relationship study that applied comparative molecular field analysis (CoMFA) methodology. Several CoMFA models were developed (variable alignments and options), and the best predictive one yields good statistical results ( $q^2 = 0.744$ ,  $r^2 = 0.891$ , and  $s = 0.273$ ). The resulting CoMFA contour maps were used to illustrate the pharmacomodulations relevant to the biological activities in this series of analogs and to design new active inhibitors. This novel series of 2,2'-bithienyl derivatives gives new insights into the design of AANAT inhibitors.

### INTRODUCTION

Melatonin is a hormone produced predominantly by the pineal gland.<sup>1,2</sup> Extra pineal sites of melatonin production include the retina,<sup>3</sup> Harderian gland,<sup>4</sup> gut,<sup>5</sup> bone marrow,<sup>6</sup> and skin.<sup>7</sup> The enzyme pathway from tryptophan to melatonin was identified many years ago and involves 5-hydroxylation by tryptophan hydroxylase, decarboxylation by aromatic-L-amino acid decarboxylase, acetylation by arylalkylamine *N*-acetyl transferase (AANAT), and finally 5-methylation by hydroxyindole-*O*-methyltransferase (HIOMT).<sup>8</sup> Studies in both the pineal gland and the retina indicate that there is a highly conserved relationship between melatonin synthesis and AANAT activity. Actually, AANAT is considered the most important enzyme for the rhythm of melatonin synthesis, since its activity is greatly enhanced at night in both tissues.<sup>9</sup>

Melatonin plays important roles in many biological processes, especially in circadian rhythms and in seasonal reproduction.<sup>10–12</sup> Melatonin pharmacology is, therefore, an important field of investigation, with the aim of trying, on one hand, to understand the mechanisms by which the hormone exerts its multiple roles, and on the other hand, to discover and assess new molecules that will permit modulating melatonin functions. Besides the classical search of agonists and antagonists of the melatonin receptors,<sup>13,14</sup> the

control of the levels of circulating melatonin represents also a major target for the search of inhibitors. Thus, AANAT has received wide attention during past years.

Inhibitors of AANAT would be useful for delineating the role of melatonin in circadian rhythms and in its other proposed but more controversial effects on aging, cancer, cardiovascular function, and the immune system.<sup>1,15,16</sup> No AANAT inhibitor with potent *in vivo* activity has been reported. Specific inhibitors of AANAT could potentially serve as therapeutic agents for alleviating sleep and mood disorders, both by raising serotonin and reducing melatonin production.<sup>17,18</sup>

Up to now, five classes of AANAT inhibitors have been described in the literature (see Zheng and Cole for a detailed review).<sup>19</sup> In brief, these five classes correspond to:

**Melatonin Derivatives.** Since it was reported that melatonin is a competitive AANAT inhibitor, this hormone seems to exert an autoregulatory control on its own biosynthesis. Thus, loose structural analogues of the indolamine hormone were evaluated on AANAT, and moderate inhibitors were discovered.<sup>20</sup>

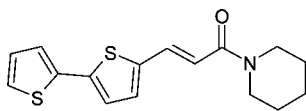
**Peptidic Inhibitors.** Ferry et al. reported the discovery of tetrapeptides coming from the deconvolution of combinatorial libraries.<sup>21</sup>

**Bisubstrate Analogs.** It is suggested that AANAT catalyzes the transfer of an acetyl group from acetylcoenzyme A (acetyl-CoA) to serotonin, with the involvement of an intermediate ternary complex, to produce *N*-acetylserotonin. Based on this mechanism, it might be expected that a bisubstrate analog inhibitor, derived from the tethering of

\* Corresponding author. Telephone: (33)2-31-56-68-22. Fax: (33)2-31-56-68-03. E-mail: alban.lepailleur@unicaen.fr.

<sup>†</sup> Centre d'Etudes et de Recherche sur le Médicament de Normandie.

<sup>‡</sup> Laboratoires Servier.



1 (Tripos 24-00037)

Figure 1. The first 2,2'-bithienyl *hit*.

indole and CoASH parts, could potentially mimic the ternary complex and exert strong inhibition of AANAT.<sup>22</sup> As anticipated, the first bisubstrate analog inhibitor, designed by Khalil and Cole,<sup>23</sup> is a very potent AANAT inhibitor ( $IC_{50} = 150$  nM). Subsequently, several bisubstrate analog inhibitors have been designed.<sup>24,25</sup>

**N-Haloacetylated Derivatives.** Besides catalyzing the acetyl transfer reaction from acetyl-CoA to serotonin to form *N*-acetylserotonin, AANAT was also demonstrated to exert a secondary alkyltransferase activity.<sup>24</sup> *N*-Haloacetyltryptamines were developed based on the pharmacological exploitation of AANAT's alkyltransferase activity.<sup>24,26</sup> AANAT catalyzes the reaction between these compounds and CoASH to form the inhibitory species, i.e., the bisubstrate analogs. With the same idea, other *N*-haloacetylated derivatives were developed as precursors of potent bisubstrate inhibitors. Some of them exhibited high inhibitory activity.<sup>27,28</sup>

**Rhodanine-based Compounds.** More recently, a new AANAT inhibitor class containing a rhodanine scaffold was described.<sup>29</sup> These derivatives, resulting from a high-throughput docking, exhibited low-micromolar competitive inhibition against acetyl-CoA and proved to be effective in blocking melatonin production in pineal cells.

While embarking on an effort to develop nonpeptidic AANAT inhibitors, we applied a medium-throughput screening (MTS) campaign on a chemolibrary commercialized by Tripos (2500 compounds). The 2,2'-bithienyl derivative **1** (Tripos 24-00037, Figure 1) emerged as a first *hit*, and structure-activity relationships were derived. A docking approach was conducted and gave insights into the plausible interactions between the new series of inhibitors and the AANAT binding site. The docking process used the Glide software<sup>30</sup> and exploited a reported X-ray structure of AANAT in complex with a bisubstrate analog.<sup>31</sup> To complete the study, a three-dimensional quantitative structure-activity relationship (3D-QSAR) study which applied comparative molecular field analysis (CoMFA) methodology,<sup>32</sup> including the steric and electrostatic fields, was also carried out in order to obtain a predictive model from a selection of 43 2,2'-bithienyl derivatives. The model was used to illustrate the pharmacomodulations relevant to the biological activities and to design new AANAT inhibitors.

## RESULTS AND DISCUSSION

**Identification of Lead Scaffold and Structure-Activity Relationships.** Compound **1** (Tripos 24-00037, Figure 1), a commercially available compound, was identified during a MTS campaign (2500 compounds) as an inhibitor of AANAT. The micromolar activity ( $IC_{50} = 0.64$   $\mu$ M) and the chemical original nature of **1** led us to consider this compound as a good initial *hit*.

At first, we realized the synthesis of 1-[(2*E*)-3-(2,2'-bithien-5-yl)prop-2-enyl]piperidine **1** in order to confirm the observed activity. Since the pharmacological results of

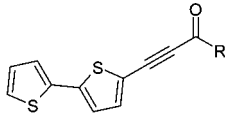
the *trans*-Tripos 24-00037 did not give the expected results ( $IC_{50} = 2.1$   $\mu$ M), the synthesis of the *cis* isomer was carried out. Only *cis/trans* mixtures were obtained (60/40 and 70/30 for the relative proportions), and their pharmacological evaluation showed comparable affinities ( $IC_{50} = 2.4$  and 4.6  $\mu$ M, respectively). Due to the interesting rigidified scaffold of the byproduct **7**, in comparison with **1**, we also evaluated its AANAT activity. With compound **7**, not only the ambiguity on the *cis/trans* isomer was put aside but also the AANAT inhibitory potency was enhanced ( $IC_{50} = 0.6$   $\mu$ M).

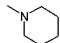
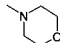
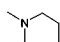
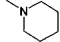
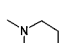
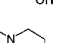

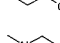
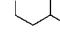
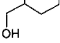
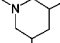
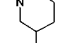
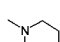
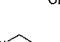
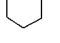
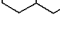
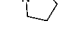
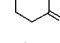
Starting from the new *lead* **7**, small groups such as methyl were appended to the piperidine ring and were generally tolerated (**10–13**, Table 1). Moreover, replacing the piperidine moiety with a decahydroquinoline (**14**), a pyrrolidine (**15**), or an azepane (**16**) retained affinity. The replacement of the piperidine with a thiomorpholine (**17**) or a morpholine (**18**) also caused no change in affinity but seems to improve the potency on the cellular model. To continue exploring the structure-activity relationships of the piperidine moiety, a number of polar groups were incorporated (**19–26**). In general, these compounds retained affinity compared to the piperidine derivatives **7**, but the most important result was their cellular potency improvement.

Among the 2,2'-bithienyl compounds synthesized during our AANAT inhibitor program, the structure-activity relationships derived from the piperazine class are relatively evident (Table 2). Indeed, the *ortho* substitutions on the phenyl piperazine moiety (**29** and **35**) seem to be favored, since the *meta* and *para* substitutions resulted in a degradation of affinity (**30–34**, **36**, and **37**). However, even if compounds **27**, **28**, and **38** retained affinity compared to the piperidine class, they showed a loss of cell-based potency.

To assess the influence of the piperidine or the piperazine moiety, new 2,2'-bithienyl derivatives carrying a secondary or tertiary amine (not included in a ring) were also prepared (Tables 3 and 4). First, varying the substituents in this position suggested that tertiary amines slightly improved affinity compared with secondary amines. Second, incorporation of larger hydrophobic substituents on such an amine seems to result in a drop in affinity. To continue exploring the structure-activity relationships of these analogues, hydroxyl groups were introduced and gave no significant variation in the  $IC_{50}$  values, excepting for compound **64** in comparison with compound **56**.

**X-ray Data.** The solved crystal structure, corresponding to compound **7**, showed that the thiophene rings are situated in a *trans* position and that the sulfur atoms lie on opposite side of the molecule (Figure 2). The two thiophene rings are slightly deviated from a coplanar position, since an angle of about 17.9(1)° is observed between the planes of the rings. The atoms of the triple bond are approximately coplanar with the neighboring thiophene ring, an angle of about 6.1(1)° is observed between the plane of the triple bond (the plane was fitted through C9–C12 atoms) and the plane of the neighboring thiophene ring. The piperidine ring is in a chair conformation and is situated up with respect to the remaining part of the molecule. In addition, the C=O bond is oriented down. The deviation of the N14 atom is about 0.73 Å with respect to the triple-bond plane, and the O13 deviation is about 0.66 Å. The deviation of the C=O from the plane of the thiophenes can be explained by a hydrogen (H)-bond-type interaction, which occurs between the O13 and the

**Table 1.** Structure–Activity Relationships around the Piperidine and Related Derivatives


	R	Pure hAANAT	hAANAT-expressing cells		R	Pure hAANAT	hAANAT-expressing cells
		IC <sub>50</sub> (μM)	IC <sub>50</sub> (μM)			IC <sub>50</sub> (μM)	IC <sub>50</sub> (μM)
7		0.6	>100	18		2.3	9.7
10		2.8	>100	19		0.9	11.2
11		2.7	>100	20		0.3	ND
12		8.2	>100	21		1.1	17.2
13		0.7	19	22		0.6	ND
14		0.4	>100	23		2.2	ND
15		2.2	>100	24		11.3	ND
16		0.6	40	25		0.5	18
17		5.1	5.0	26		2.5	22.7

C8–H8 of a neighboring molecule (1 + x, y, z). The distance between O13 and H8 is about 2.29 Å.

In the crystal packing, beside the already described interaction O···H–C, stacking interaction occurs between the thiophene rings of two neighboring molecules along the *b* axis. The distance between the thiophene ring planes of neighboring molecules is about 3.69 Å.

**Molecular Docking Studies.** Molecular modeling studies were initiated in order to probe the possible interactions between compound **7** and AANAT. The X-ray coordinate system used for these studies corresponds to 1CJW, a high-resolution structure of AANAT in which a bisubstrate analog is bounded at the enzyme active site.<sup>31</sup> The bisubstrate analog mimics the structure of the presumed intermediate formed during catalysis and was first described by Khalil and Cole.<sup>23</sup> The analog is held in a conformation that is approximately “S”-shaped (Figure 3). The pantetheine group is aligned parallel to strand β5 of the central β sheet, held in place by a number of H-bonding contacts involving main chain atoms (Leu124 and Val126). The α- and β-phosphates of the adenosine diphosphate (ADP) group also form several H-bonds with AANAT residues (Gln132, Gly134, Gly136, and Ser137). On the opposite side, the indole ring of the tryptamine group is held in place through extensive hydrophobic contacts with six residues (Phe56, Pro64, Met159, Val183, Leu186, and Phe188), which converge to form a pocket, referred to as the serotonin binding site.

As explained in the Experimental Section, compound **7** was docked into the binding site of AANAT using the SP

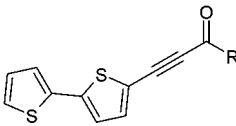
Glide methodology. Among the two H-bond constraints defined during the receptor grid generation step, at least one of them had to be achieved (with the main chain amide of Leu124 or the water molecule 1061). These constraints were chosen because they are situated at the junction between the AcCoA and the serotonin binding sites, where the carbonyl group of compound **7** is supposed to be. The docking results led us to the consideration of three different positions (Figures 4–6). First, and as initially envisaged, the bithienyl moiety could occupy the AcCoA binding site, leading to the positioning of the piperidine group in the serotonin binding pocket. In this case, two orientations can be observed for the carbonyl group of the ligand, depending on the H-bond constraint which is filled (Figures 4 and 5). In order to determine the accuracy of this prediction, the piperidine group of **7** was replaced by a tryptamine moiety, and the inhibitory potency of the new compound **50** was evaluated (Table 3). The pharmacological results showed that the introduction of the tryptamine moiety causes a loss of AANAT inhibitory activity (IC<sub>50</sub> > 100 μM). As a consequence, this single synthetic change to the derivative **7** suggested that the bithienyl moiety should occupy the serotonin binding pocket rather than the AcCoA binding site, as highlighted by the third docking possibility (Figure 6). Molecular docking studies also demonstrated that the carbonyl oxygen of **7** is not able to form a H-bonding contact with the main chain amide of Leu124 when the bithienyl moiety occupies the serotonin binding pocket. The resulting position involves two water-mediated H-bonds with both the

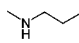
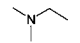
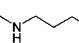
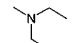
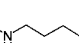
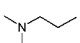
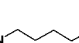
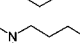

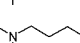
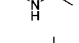
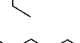
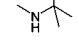
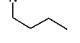
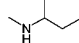

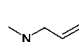
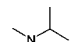

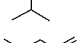
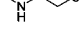
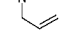
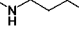
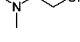
**Table 2.** Structure–Activity Relationships around the Piperazine and Related Derivatives

	R	Pure hAANAT	hAANAT-expressing cells		R	Pure hAANAT	hAANAT-expressing cells
		IC <sub>50</sub> (μM)	IC <sub>50</sub> (μM)			IC <sub>50</sub> (μM)	IC <sub>50</sub> (μM)
27		3.7	>100	34		>100	ND
28		8.9	>100	35		9.3	ND
29		47	ND	36		25.2	ND
30		>100	ND	37		>100	ND
31		>100	ND	38		2.9	>100
32		>100	ND	39		39.5	ND
33		>100	ND	40		16	ND

**Table 3.** Structure–Activity Relationships around the Secondary and Tertiary Amine Derivatives (Carrying a Ring)

	R	Pure hAANAT	hAANAT-expressing cells		R	Pure hAANAT	hAANAT-expressing cells
		IC <sub>50</sub> (μM)	IC <sub>50</sub> (μM)			IC <sub>50</sub> (μM)	IC <sub>50</sub> (μM)
41		>100	ND	48		6.3	ND
42		0.8	>100	49		>100	ND
43		1.5	>100	50		>100	ND
44		9.3	>100	51		0.5	56
45		>100	ND	52		0.6	>100
46		>100	ND	53		0.6	37
47		0.3	ND				

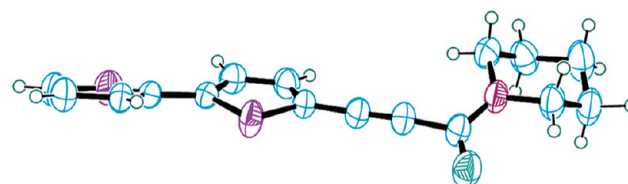
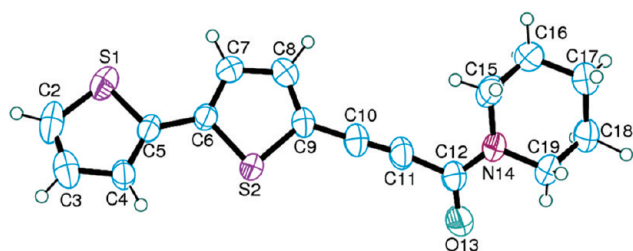
**Table 4.** Structure–Activity Relationships around the Secondary and Tertiary Amine Derivatives (Not Carrying a Ring)


	R	Pure hAANAT	hAANAT-expressing cells		R	Pure hAANAT	hAANAT-expressing cells
		IC <sub>50</sub> (μM)	IC <sub>50</sub> (μM)			IC <sub>50</sub> (μM)	IC <sub>50</sub> (μM)
54		>100	ND	66		5.0	>100
55		4.2	ND	67		1.8	>100
56		>100	ND	68		1.6	>100
57		>100	ND	69		6.0	>100
58		>100	ND	70		0.6	19
59		>100	ND	71		1.1	>100
60		7.3	>100	72		>100	ND
61		0.9	18	73		6.1	>100
62		>100	ND	74		0.5	12
63		>100	ND	75		12	ND
64		5.1	25	76		1.5	21.9
65		>100	ND	77		1.3	12.8

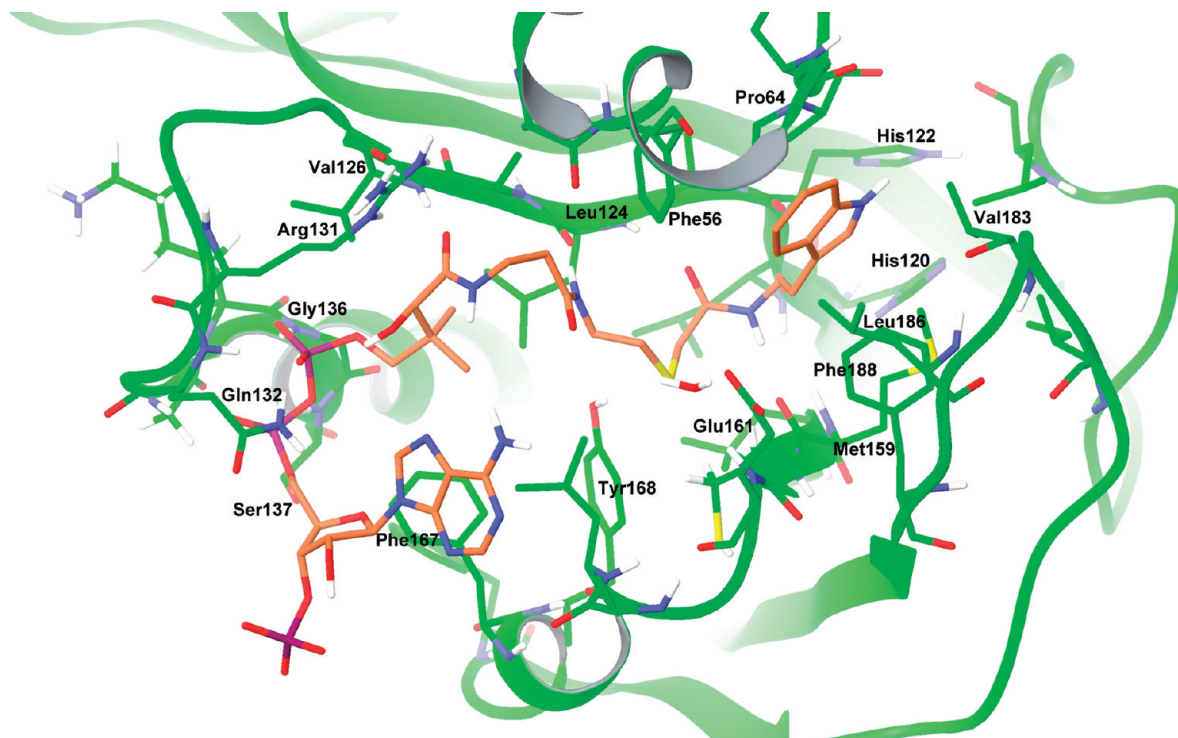
main and side chains of Glu161. Besides, the bithienyl moiety fills the hydrophobic funnel that led directly toward His120 and His122, which are involved in the catalytic mechanism.<sup>31</sup> To go even further, we can postulate that the beneficial effect observed with the introduction of polar groups could result from H-bond contacts with Leu124, Val126, and/or Arg131. This hypothesis is strengthened by the widely different activities observed for compounds **20** vs **12** and **19** vs **11**. With the same idea, we can assume that the better activity observed for compound **64**, in comparison with compound **56**, is due to an effect of a H-bond. In fact, these compounds differentiate only by the addition of a hydroxyl group. In addition, the lower activity of compound **63**, when compared with compound **20**, seems to indicate that a precise conformation is mandatory. This difference could result from the formation of an intramolecular H-bond, preventing a H-bond contact with Val126 and/or Arg131. The same result can be deduced from compound **62**. Moreover, compounds **75–77**

also support this hypothesis, since their higher affinity is coupled with the presence of a tertiary amine, which avoid the undesired folding behavior of the hydroxylated chain. By considering the phenyl piperazine derivatives, the H-bond constraint with the main chain amide of Leu124 could not be achieved (data not shown). Consequently, the solvent exposure of the carbonyl group of these bithienyl derivatives is highly plausible, and a water network could mediate H-bond interactions with polar residues such as Glu161.

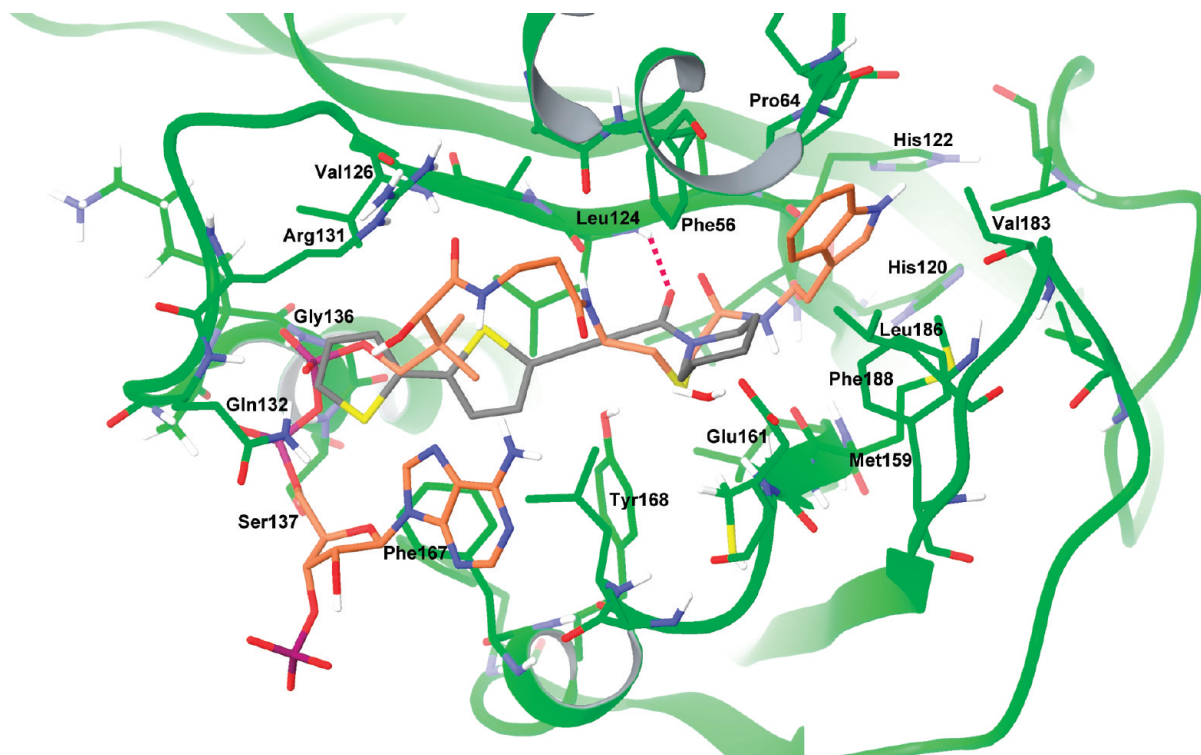
**CoMFA Studies.** Even though the docking studies gave insights into the binding mode possibilities for the bithienyl derivatives, uncertainties remain. Thus, we realized a 3D-QSAR study which applied the CoMFA methodology in order to better understand the relations between the pharmacomodulations and the biological activities in this series of analogs. The compounds, referenced in Table 9, were selected as a training set, and their capacity to inhibit AANAT was expressed in terms

**Figure 2.** X-ray crystal structure of compound **7**.





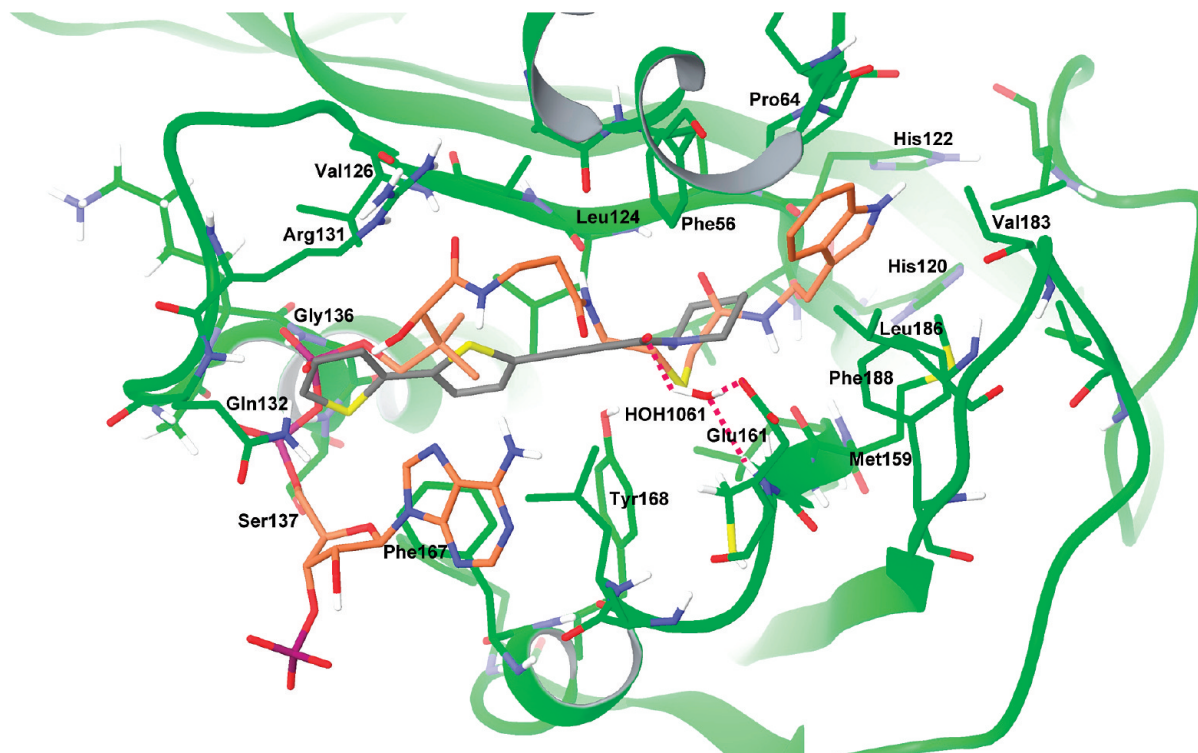
**Figure 3.** AANAT-bisubstrate analog complex (PDB code 1CJW).



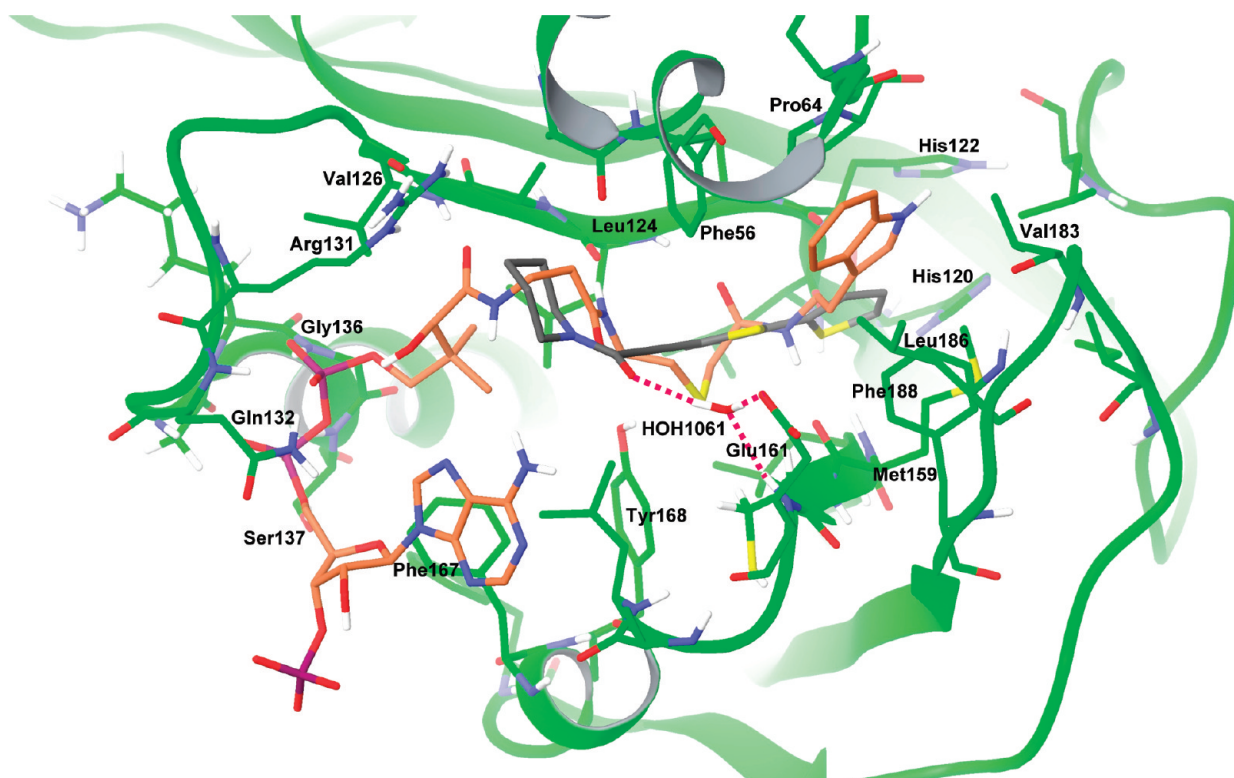
**Figure 4.** Comparison between the first docking position (in gray) and the bisubstrate binding mode (in orange).

of  $pIC_{50}$  or  $-\log(IC_{50})$ , where  $IC_{50}$  represents the drug concentration that inhibits 50% of pure AANAT activity. The  $pIC_{50}$ , which covers four logarithmic units, was used as a dependent variable in the CoMFA calculations. For these studies, the selection of the training set compounds was influenced, on one hand, by the availability of the  $IC_{50}$  values and, on the other hand, by the presence/absence of a stereocenter. Indeed, the compounds which exhibited a stereocenter were put aside, since their consideration increased the complexity of the crucial alignment step.

All compounds were initially aligned on the X-ray crystallographic structure of **7** (Figure 2). The fitting processes were achieved according to selected pairs of atoms, using a SPL program. The fixed atoms corresponding to the template are represented by the entire molecule **7**, excepting atoms C15–C19 (Figure 2). Concerning the geometries of the remaining moieties for the training set molecules, the structural information we collected on the Cambridge Structural Database (CSD)<sup>33</sup> led us to uncertainties. Consequently, we had to propose four different



**Figure 5.** Comparison between the second docking position (in gray) and the bisubstrate binding mode (in orange).

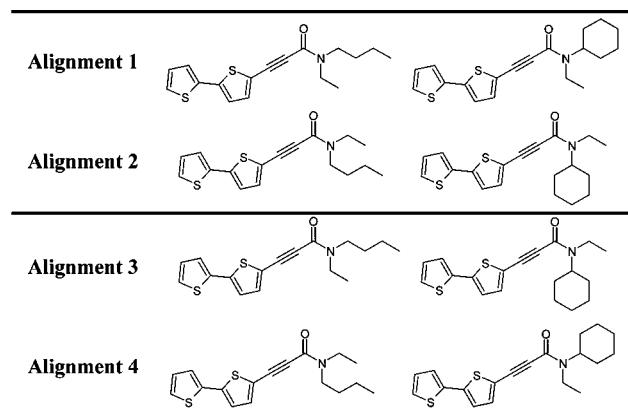


**Figure 6.** Comparison between the third docking position (in gray) and the bisubstrate binding mode (in orange).

alignments. Table 5 presents examples that illustrate these various possibilities.

First of all, we searched the optimal alignment by considering the CoMFA default parameters ("smooth" option). The statistical results obtained with all alignments are recapitulated in Table 6. The CoMFA analyses were initially performed with probe atoms placed on a regularly spaced grid of 2 Å. No significant differences were observed

between the statistical results. These results indicated the good predictive capacity of the models, which yielded a cross-validated correlation coefficient  $q^2$  from 0.549 to 0.728, with reasonable respective standard errors of prediction  $SE_{cv}$  (from 0.550 to 0.432). As just noted, a  $q^2$  value of 0.3 corresponds to a 95% confidence limit, which minimizes the risk of chance correlation.<sup>34</sup> These analyses were then repeated with a grid of 1 Å because, according to Cramer,<sup>32</sup>

**Table 5.** Representation of the Four Alignment Possibilities

this operation achieves a quality improvement of sampling. As anticipated, the diminution of the grid spacing improves the results.

Since all alignments exhibited comparable performances, we decided to carry out our studies with the third one (Figure 7), which presented slightly better  $q^2$  and  $SE_{cv}$  values.

As mentioned above, these models have been generated with the default “smooth” option. However, other methods of field generation are available to users of CoMFA, and in some cases, better models could be obtained.<sup>35</sup> Thus, the influences of these three methods were studied for the third alignment. It should be noted that for these analyses, the “box” option yielded worse results than both the “smooth” and “abrupt” options (Table 7). Finally, we retained the model generated from the “abrupt” method.

The complete statistical results are recapitulated in Table 8. Using the optimal number of components (3), the nonvalidated model was produced and led to satisfying the correlation coefficient  $r^2$  (0.891) and the standard error of estimate  $SE_E$  (or  $s$ , 0.273). These data suggested a good correlation between the steric and electrostatic molecular fields and the activities measured for the training set. The contributions were 67% for the steric fields and 33% for the electrostatic fields (final equation). The experimental vs predicted activity values for the final model (without cross-validation) are presented in Figure 8 and in Table 9. The plot of residuals for the data set is shown in Figure 9.

Graphic representation of the CoMFA model is displayed in Figure 10. It shows regions where variations of steric or electrostatic nature in the structural features of the training set compounds lead to variations of activity. Green contours indicate regions where an increase of steric bulk will enhance activity, whereas yellow contours indicate regions where an increase of steric bulk will reduce activity. Regions where an electrostatic interaction is favorable for activity are indicated in blue, while regions where an electrostatic interaction is detrimental for activity are indicated in red.

Within the training set, few inhibitors are able to occupy simultaneously the two regions corresponding to favorable steric bulks (fields **a** and **b**, Figure 11). Compound **53** (Table 3) is one of them, and this characteristic enables it to belong to the best-predicted compounds (Table 9).

The region where an increase of steric bulks will reduce activity primarily interests the piperazine derivatives related to inhibitor **28** (Table 2). This region highlights the detrimental effect of *meta* (**30**, **34**, and **36**) and *para* (**31**, **33**, and

**37**) substitutions on the phenyl ring. On the contrary, *ortho* substituents seem to be tolerated (**29** and **35**).

With regard to the contour maps of the favorable electrostatic fields, a moderate increase of activity could be achieved by incorporating polar groups. Particularly, these favorable substitutions are exemplified by compounds **20** and **25**. This graphic representation can also be illustrated with compound **38** (Figure 12). Among the inhibitors presenting a piperazine moiety, **38** is the most potent. According to the CoMFA results, its C1–N2–C3–N4 torsion angle ( $140^\circ$ ) leads to a correct orientation of the pyridinyl ring, with regard to the favorable electrostatic area (field **e**, Figure 12). It results in a slight increase of activity in comparison with compound **28**.

Using the comparative molecular similarity indices analyses (CoMSIA)<sup>36</sup> program, an approach related to the CoMFA analysis, we added hydrophobic parameters to our 3D-QSAR equation. Since this additional information did not lead to a significant improvement of the model, the CoMSIA approach was put aside.

**CoMFA-Based Pharmacomodulations.** To validate and complete our model, we proposed the synthesis of new compounds, and we attempted to predict their activities. These propositions started with **48** which exhibits a first affinity and an interesting aromatic cycle, in view of the envisaged pharmacomodulations. Indeed, due to the position of the phenyl ring, appropriate substitutions could lead to a good occupancy of the previously discussed favorable steric regions.

The predicted and experimental  $pIC_{50}$  values for the six new compounds (**78**–**83**) are specified in the Table 10. Clearly, their activities are overestimated but are generally comparable to those of the *lead* compounds. Besides, we have highlighted the harmful effect of a *meta* substitution on the phenyl (**81** and **82**). Finally, we proposed a compound which exhibits a tertiary amine substituted not only by a phenyl ring but also by an allyl chain. The pharmacomodulation was suggested by the promising compounds **61** and **74**, which combine good activities on pure enzyme and cellular models (Table 4). The resulting derivative **83** retained affinity in comparison with the best ones.

## CONCLUSION

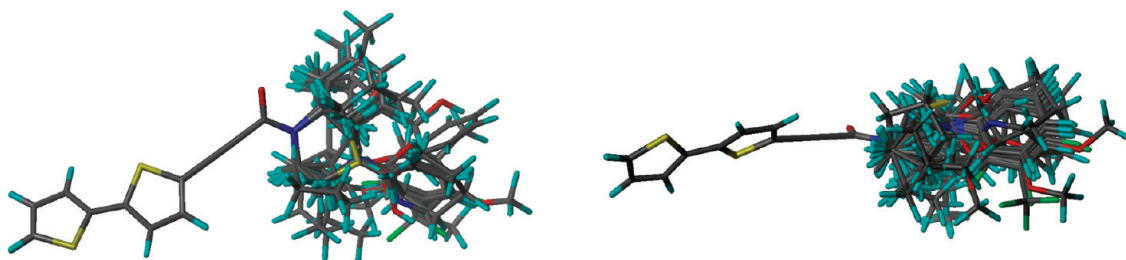
This study initially describes the discovery of a new class of nonpeptidic AANAT inhibitors based on a 2,2'-bithienyl scaffold. Compound **1** emerged from a medium-throughput screening campaign performed on a chemolibrary commercialized by Tripos. Structure–Activity relationships were derived and led to a first *lead*, compound **7**, whose interesting rigidified scaffold attracted our attention. Afterward, molecular modeling studies were initiated in order to probe the possible interactions between compound **7** and AANAT. First, docking studies pointed to three plausible binding modes for this new AANAT inhibitor. The most promising one suggested that the bithienyl moiety should occupy the serotonin binding pocket and that the carbonyl oxygen should be involved in water-mediated H-bonds with the main and side chains of Glu161. Besides, in this case, the bithienyl moiety should fill the hydrophobic funnel that led directly toward the His120 and His122, which are involved in the catalytic mechanism. Second, and in order to better understand the relations between the pharmacomodulations and



**Table 6.** Statistical Results for the Four Possible Alignments<sup>a</sup>

alignment	grid, Å	ONC	$q^2$	SE <sub>cv</sub>	$r^2$	SE <sub>E</sub> (s)	steric contribution, %	electrostatic contribution, %
<b>1</b>	2	2	0.588	0.525	0.780	0.384	76	24
	1	3	0.712	0.445	0.894	0.270	66	34
<b>2</b>	2	2	0.580	0.531	0.778	0.386	75	25
	1	3	0.708	0.448	0.896	0.267	70	30
<b>3</b>	2	2	0.607	0.513	0.767	0.395	77	23
	<b>1</b>	<b>3</b>	<b>0.728</b>	<b>0.432</b>	<b>0.891</b>	<b>0.274</b>	<b>67</b>	<b>33</b>
<b>4</b>	2	2	0.549	0.550	0.796	0.369	73	27
	1	3	0.688	0.463	0.902	0.260	70	30

<sup>a</sup> ONC is the optimal number of components,  $q^2$  is the cross-validated correlation coefficient, SE<sub>cv</sub> is the standard error of prediction,  $r^2$  is the correlation coefficient, and SE<sub>E</sub> is the standard error of estimate.

**Figure 7.** Selected alignment (number three).**Table 7.** Additional Statistical Results for Alignment Three

method	grid, Å	ONC	$q^2$	SE <sub>cv</sub>	$r^2$	SE <sub>E</sub> (s)	steric contribution, %	electrostatic contribution, %
smooth	2	2	0.607	0.513	0.767	0.395	77	23
	1	3	0.728	0.432	0.891	0.274	67	33
abrupt	2	2	0.595	0.521	0.767	0.395	77	23
	<b>1</b>	<b>3</b>	<b>0.744</b>	<b>0.420</b>	<b>0.891</b>	<b>0.273</b>	<b>67</b>	<b>33</b>
box	2	3	0.603	0.522	0.874	0.294	68	32
	1	2	0.676	0.466	0.797	0.368	75	25

**Table 8.** Final Results of the CoMFA Analysis for Alignment Three<sup>a</sup>

cross-validation			final equation	
number of components	$q^2$	SE <sub>cv</sub>	$r^2$	SE <sub>E</sub> (s)
1	0.565	0.533		
2	0.720	0.433		
<b>3</b>	<b>0.744</b>	<b>0.420</b>	<b>0.891</b>	<b>0.273</b>
4	0.740	0.428		
5	0.744	0.431		
6	0.733	0.446		

<sup>a</sup> With 1 Å spacing and with the “abrupt” method.

the biological activities in this series of analogues, we realized a 3D-QSAR study that applied CoMFA methodology. The best predictive model yields good statistical results ( $q^2 = 0.744$ ,  $r^2 = 0.891$ , and  $s = 0.273$ ), and the resulting contour maps were used to design new inhibitors with micromolar activity.

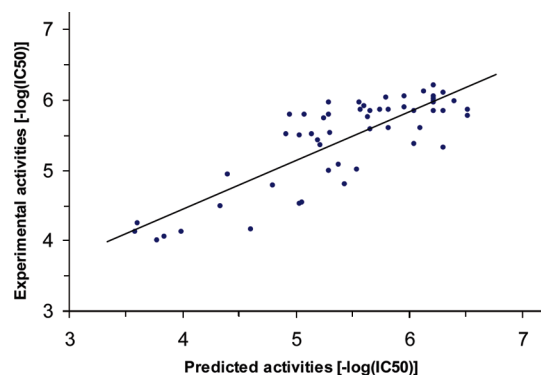
To complete the study, 18 representative compounds were selected among all our 2,2'-bithienyl derivatives, and their affinities for MT1 and MT2 melatonergic receptors were evaluated according to Audinot et al.<sup>45</sup> Satisfying results were observed since all of them showed a  $K_i$  greater than 10  $\mu$ M (unpublished data).

To conclude, this work gives new insights into the design of nonpeptidic AANAT inhibitors. Besides, the selection of the morpholine derivative, **18** as a new *lead*, was encouraged

by its chemical structure and its potency on the cellular model. Presently, supplementary pharmacological evaluations are ongoing, and synthetic experimental details will be described elsewhere.

## EXPERIMENTAL SECTIONS

**Chemistry.** The synthesis of **1** started from 2-bromothiophene (Scheme 1). The formation of 5-bromo-2,2'-bithiophene **2** or 5-iodo-2,2'-bithiophene **3** derivatives<sup>37,38</sup> were obtained in good yields. The synthesis of methyl (2E)-3-(2,2'-bithien-5-yl)acrylate **4** was prepared by a palladium-catalyzed coupling with methyl acrylate under phase-transfer

**Figure 8.** Plot of the experimental vs predicted  $pIC_{50}$  values (without cross-validation).

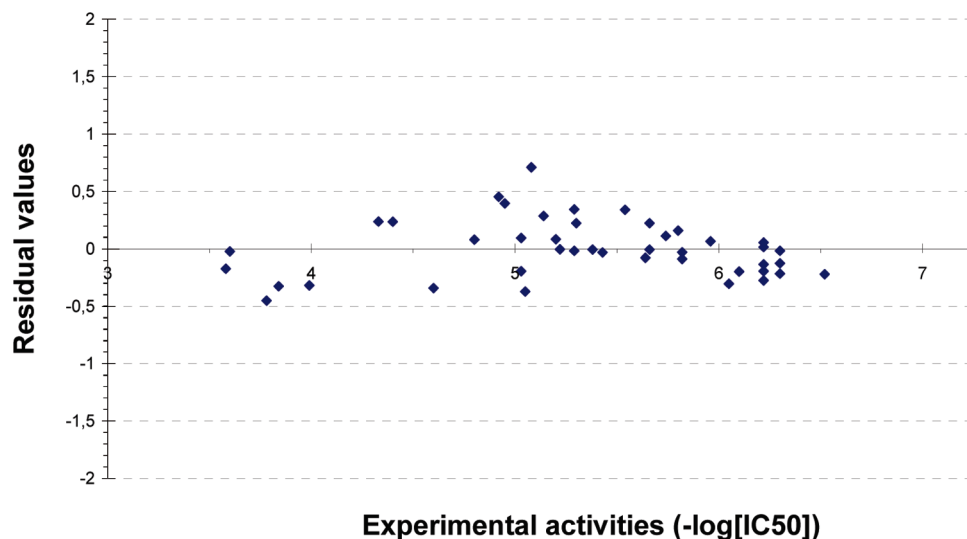


Figure 9. Plot of the residual values (without cross-validation).

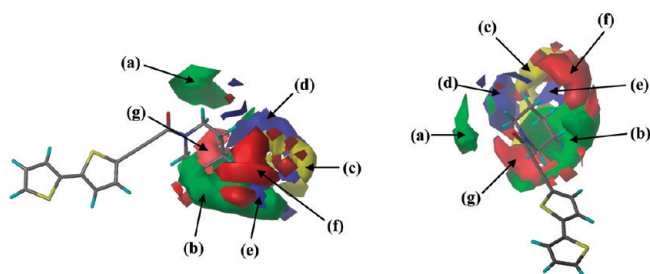


Figure 10. Standard deviation \*PLS coefficients contour plots of CoMFA steric and electrostatic fields (green: favorable steric bulks **a** and **b**; yellow: detrimental steric bulk **c**; blue: electrostatic favored areas **d** and **e**; and red: electrostatic disfavored areas **f** and **g**). Compound **7** inside the map.

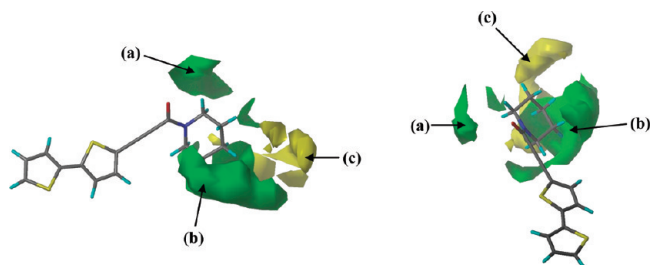


Figure 11. Standard deviation \*PLS coefficients contour plots of CoMFA steric fields (green: favorable steric bulks **a** and **b**; and yellow: detrimental steric bulk **c**). Compound **7** inside the map.

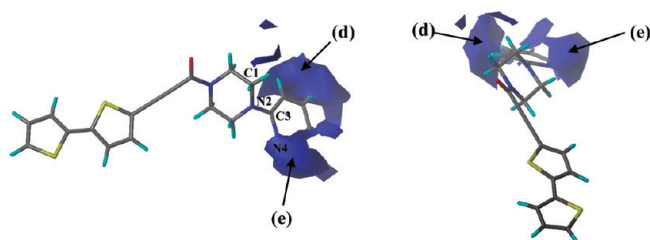


Figure 12. Standard deviation \*PLS coefficients contour plots of CoMFA favorable electrostatic areas. Compound **38** inside the map.

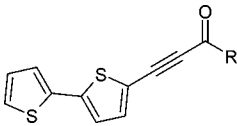
conditions.<sup>39</sup> The formation of acid (2*E*)-3-(2,2'-bithien-5-yl)acrylic was obtained by saponification of the ester, and finally compound **1** was achieved by substitution of the mixed anhydride with piperidine.

Table 9. Experimental vs Predicted Values for the Final Model<sup>a</sup>

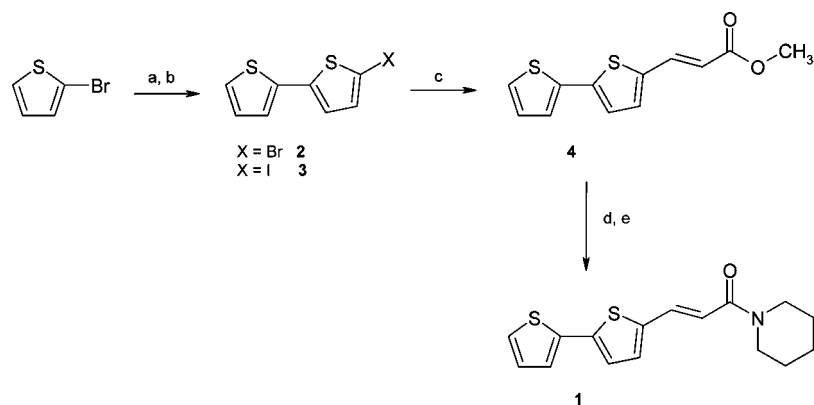
no.	experimental $pIC_{50}$	predicted $pIC_{50}$	difference
7	6.22	5.85	0.37
12	5.08	5.82	-0.74
15	5.66	5.62	0.04
16	6.22	5.99	0.23
17	5.29	5.64	-0.35
18	5.64	5.53	0.11
20	6.52	6.17	0.35
23	5.66	5.85	-0.19
24	4.95	5.39	-0.44
25	6.30	6.07	0.23
27	5.43	5.39	0.04
28	5.05	4.71	0.34
29	4.33	4.68	-0.35
30	3.99	3.82	0.17
31	3.58	3.60	-0.02
33	3.60	3.77	-0.17
34	3.84	3.68	0.16
35	5.03	4.87	0.16
36	4.60	4.34	0.26
37	3.78	3.50	0.28
38	5.54	5.86	-0.32
39	4.40	4.74	-0.34
40	4.80	4.94	-0.14
42	6.10	5.82	0.28
43	5.82	5.74	0.08
44	5.03	5.16	-0.13
48	5.20	5.30	-0.1
51	6.30	6.18	0.12
52	6.22	6.14	0.08
53	6.22	6.18	0.04
55	5.38	5.37	0.01
60	5.14	5.45	-0.31
61	6.05	5.67	0.38
64	5.29	5.28	0.01
66	5.30	5.53	-0.23
67	5.74	5.81	-0.07
68	5.80	5.91	-0.11
69	5.22	5.23	-0.01
70	6.22	5.93	0.29
71	5.96	5.96	0.00081
73	6.30	5.98	0.32
74	4.92	5.42	-0.5
75	5.82	5.68	0.14

<sup>a</sup> Without cross-validation.

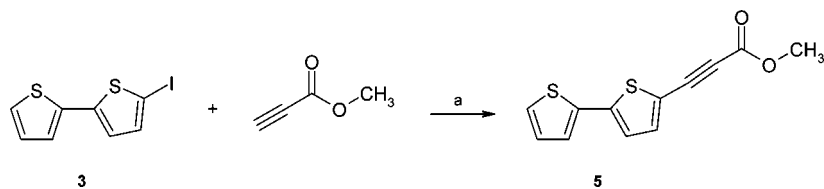
Another way of synthesis was, thus, envisaged to obtain the *cis* product. This method consists, first of all, in realizing

**Table 10.** Experimental vs Predicted Values for the New Proposed Inhibitors


Num.	R	Experimental $pIC_{50}$	Predicted $pIC_{50}$	Difference
48		5.20	5.30	-0.10
78		5.72	6.20	-0.48
79		5.54	6.41	-0.87
80		5.74	6.65	-0.9
81		<4	6.35	-
82		<4	6.39	-
83		5.92	6.57	-0.65

**Scheme 1.** Synthesis of 1-[(2E)-3-(2,2'-bithien-5-yl)prop-2-en-1-yl]piperidine **1** (Tripos 24-00037)<sup>a</sup>

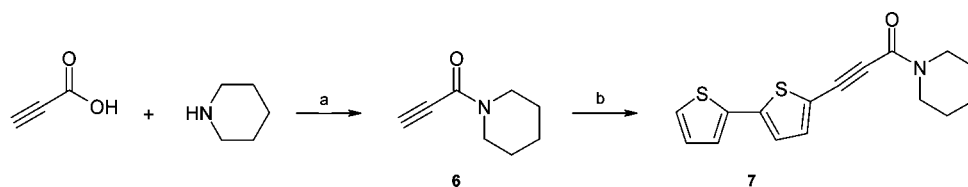
<sup>a</sup> Reagents and conditions: (a) (1) Mg, Et<sub>2</sub>O, reflux 30 min; (2) Ni(dpp)Cl<sub>2</sub>, reflux 4 h, 97%; (b) NBS or NIS, CHCl<sub>3</sub>/AcOH, room temperature, 12 h under argon, 60–70%; (c) Pd(OAc)<sub>2</sub>, NBu<sub>4</sub>I, K<sub>2</sub>CO<sub>3</sub>, methyl acrylate, DMF, 85 °C, 24 h under argon, 78%; (d) NaOH, MeOH/H<sub>2</sub>O, HCl, 85%; (e) ClCO<sub>2</sub>CH<sub>3</sub>, Et<sub>3</sub>N, acetone, piperidine, 12 h, room temperature, 68%.

**Scheme 2.** Synthesis of Methyl 3-(2,2'-Bithien-5-yl)prop-2-ynoate **5**<sup>a</sup>

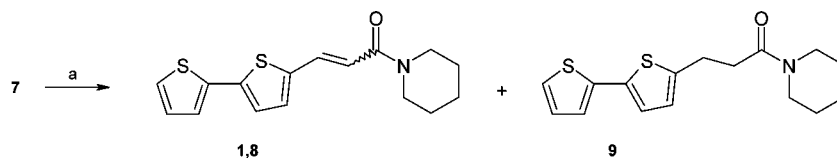
<sup>a</sup> Reagents and conditions: (a) Et<sub>3</sub>N, PdCl<sub>2</sub>(PPh<sub>3</sub>)<sub>2</sub>, CuI, THF, reflux 18 h under argon, 20%.

a coupling of Sonogashira<sup>40</sup> from the methyl propiolate with **3**. Several assays were realized with various palladium catalysts (Pd(PPh<sub>3</sub>)<sub>4</sub> and PdCl<sub>2</sub>(PPh<sub>3</sub>)<sub>2</sub>) and with various solvents, such as DMF, acetonitrile, or THF. The best results are obtained with the palladium catalyst PdCl<sub>2</sub>(PPh<sub>3</sub>)<sub>2</sub> in THF (20% yield, see Scheme 2).

Due to the low yields, we were interested in the synthesis of propiolamides **6** derivatives from propiolic acid and amines. Multiple synthetic routes were explored before optimal conditions were developed. The method involved the cross-coupling reaction of propiolamides with **3**. The product (compound **7**) was carried out at room temperature

**Scheme 3.** Synthesis of 1-[3-(2,2'-Bithien-5-yl)prop-2-ynoyl]piperidine **7**<sup>a</sup>

<sup>a</sup> Reagents and conditions: (a)  $\text{CHCl}_3$ , DCC, 0 °C, 1 h, 58%; (b) 5-iodo-2,2'-bithiophene,  $\text{Et}_3\text{N}$ ,  $\text{Pd}(\text{PPh}_3)_4$ ,  $\text{CuI}$ , DMF, room temperature, 18 h, 84%.

**Scheme 4.** Synthesis of 1,1-[(2Z)-3-(2,2'-bithien-5-yl)prop-2-enoyl]piperidine **8** and 1-[3-(2,2'-Bithien-5-yl)propanoyl]piperidine **9** derivatives<sup>a</sup>

<sup>a</sup> Reagents and conditions: (a)  $\text{H}_2$ ,  $\text{Pd}/\text{BaCO}_3$ , EtOH, room temperature, 1.5 h, 82%.

in the presence of  $\text{Pd}(\text{PPh}_3)_4$  (5 mol %),  $\text{CuI}$  (5 mol %), and triethylamine in DMF (Scheme 3). Finally, the reaction of catalytic hydrogenation<sup>41</sup> was realized in the presence of palladium on barium carbonate and quinoline in anhydrous ethanol. Only mixtures of *cis/trans* were obtained whose reports were of the order 60/40 and 30/70 (separable by chromatography) and total reduction of the compound (Scheme 4).

Afterward, we were interested in the synthesis of a byproduct possessing a triple connection and carrying different amines (secondary, tertiary, substituted piperidine or piperazine, and aniline).

**Culture of AANAT-Expressing Cell Line.** The selection of a positive clone, CHO-hAANAT-8, has been described elsewhere.<sup>42</sup> Cells were seeded ( $1 \times 10^6$  cells per well in a 96-well plate) and cultured for 72 h with 5%  $\text{CO}_2$ :95% air (v/v) in a humidified incubator in 96-well plates containing Ham 4MF12 medium (GIBCO BRL, Invitrogen SARL, Cergy-Pontoise, France) supplemented with 10% (v/v) fetal bovine serum,  $50 \mu\text{g mL}^{-1}$  penicillin/streptomycin, 2 mM L-glutamine, 5 mg  $\text{mL}^{-1}$  G418, all from Life Technologies.

**Expression and Production of hAANAT.** Expression, production, and purification of hAANAT have been described by Ferry et al.<sup>43</sup> In brief, the human arylalkylamine *N*-acetyltransferase cDNA coding five region (kindly provided by D. C. Klein and S. L. Coon, National Institutes of Health, Bethesda, MD) was inserted into the bacterial expression vector pGEX-4T (Pharmacia, Les Ulis, France), leading to the expression of a protein fused to glutathione-*S*-transferase. An *Escherichia coli* strain [BL21(DE3)pLysS] was transformed with the resulting plasmid. Expression of the construct was induced by adding isopropyl thio- $\beta$ -D-galactoside (0.2 mM) at 24 °C for 6 h. The cells were harvested by centrifugation (5000 g, 4 °C for 10 min). All purification procedures were performed at 0–4 °C. Approximately 10 g of a frozen bacteria pellet was thawed in 40 mL of  $2 \times \text{NaCl}/\text{Pi}$  containing 10 mM dithiothreitol, a cocktail of protease inhibitors (Complete, Roche; 1 tablet per 50 mL) and Tween 85 (5% v/v). This suspension was sonicated eight times for 1 min in ice, centrifuged (20 000 g, 20 min), and the supernatant passed through an affinity column  $40 \text{ mL h}^{-1}$  (glutathione-sepharose, Pharmacia), that was previously equilibrated with buffer A ( $2 \times \text{NaCl}/\text{Pi}$ , pH 6.9, containing 10 mM dithiothreitol). The column was

washed (40 mL buffer A) and then eluted with 150 mL of buffer B (50 mM Tris/HCl, pH 8.0, containing 100 nM sodium citrate, 10 mM dithiothreitol, and 10% (v/v) glycerol). The glutathione-*S*-transferase-AANAT was eluted sequentially with 40 mL of 10 mM glutathione in buffer B. Active fractions were pooled and stored frozen at 80 °C until used. The protein concentration was determined by the Bradford assay<sup>44</sup> (Protassay, Bio-Rad, Ivry-sur-Seine, France) with bovine serum albumin as the standard.

**Assays for Enzymatic and Cellular AANAT.** An enzymatic assay for AANAT was performed in a 100  $\mu\text{L}$  final volume comprising 1  $\mu\text{g}$  of enzyme, in a phosphate buffer (50 mM sodium phosphate, pH 6.8, 500 mM NaCl, and 2 mM EDTA) with 1 mM acetyl-CoA and 4 mM phenylethylamine. Compounds were dispensed in black 96-well plates (Costar, Dutscher, Issy-les-Moulineaux, France) under a volume of 10  $\mu\text{L}$ , at a starting concentration of 100  $\mu\text{M}$  in pure dimethylsulfoxide. Cellular assays for AANAT were performed on subconfluent cells seeded in 96-well plates and incubated with 10  $\mu\text{L}$  of the tritiated substrate [ $^3\text{H}$ ]phenylethylamine ([ $^3\text{H}$ ]PEA, Amersham Pharmacia Biotech, 2.78 TBq  $\text{mmol}^{-1}$ ). In brief, for cell studies, 70  $\mu\text{L}$  of incubation buffer (phosphate buffer detailed above) containing 0.5% Tween 85 were added to each well of the plates. Plates were shaken at room temperature for 30 min using an orbital shaker (Bioblock Scientific, Strasbourg, France). Each well was then sonicated once (setting 40/100, probe 0.2 cm diameter) for five seconds. For [ $^3\text{H}$ ]bromoacetyltryptamine experiments ([ $^3\text{H}$ ]BAT, Amersham-Pharmacia Biotech, 2.25 TBq  $\text{mmol}^{-1}$ ), 10  $\mu\text{L}$  of the compound was added, along with cold PEA standard incubation, to the enzyme or to the cells in 96 well plates. After incubation (30 min, 37 °C), the reaction was stopped by the addition of 50  $\mu\text{L}$  of 10% (v/v) trichloroacetic acid in water. Thirty microliters of the enzymatic reaction, conditioned culture media, or lysed cells were analyzed by reverse phase HPLC using a C4 ASTEC,  $4.6 \times 150 \text{ mm}$  column (CIL Cluzeau, Ste-Foy-la-Grande, France). The column was developed with a linear gradient of 5–35 or 0–100% (v/v) acetonitrile in  $\text{H}_2\text{O}$ , 0.1% (v/v) trifluoroacetic acid at a flow rate of 1  $\text{mL min}^{-1}$  for 15 or 30 min. The area under the peak of the reaction product was integrated by the software of the HPLC system (HP-CHEMSTATION, v06.01; Agilent Technologies, Waldbronn, Germany), by comparison of surfaces of the peak for



*N*-acetylPEA in the presence and absence of compounds. At least two determinations were made for each experiment. Each inhibition factor was calculated using the mean values of those duplicates.

**Binding Experiments at Human MT<sub>1</sub> and MT<sub>2</sub> Receptors.** Binding experiments were carried out as described previously in Audinot et al.<sup>45</sup> The CHO–K1 cell lines stably expressing either hMT<sub>1</sub> or hMT<sub>2</sub> receptors were grown at confluence, harvested in phosphate buffer containing 2 mM EDTA, and centrifuged at 1000 g for 5 min at 4 °C. The resulting pellet was suspended in 5 mM Tris/HCl, pH 7.4, containing 2 mM EDTA, and homogenized using a Kinematica (Lucerne, Switzerland) polytron. The homogenate was then centrifuged (20 000 g, 30 min, 4 °C), and the final pellet was suspended in 75 mM Tris/HCl, pH 7.4, containing 2 mM EDTA and 12.5 mM MgCl<sub>2</sub>. The determination of protein content was performed, according to Bradford,<sup>44</sup> using the Bio-Rad kit (Bio-Rad SA, Ivry-sur-Seine, France). Aliquots of membrane preparations were stored at –80 °C until further use. 2-[<sup>125</sup>I]iodomelatonin binding assay experiments were conducted as follows: membranes were incubated for 2 h at 37 °C in binding buffer (Tris/HCl 50 mM, pH 7.4, 5 mM MgCl<sub>2</sub>) in a final volume of 250  $\mu$ L containing 2-[<sup>125</sup>I]iodomelatonin (25 or 200 pM for competition experiments in MT<sub>1</sub>–CHO and MT<sub>2</sub>–CHO cells, respectively, according to the slightly better affinity of this compound to MT<sub>1</sub> as compared to MT<sub>2</sub>). Nonspecific binding was defined with 10  $\mu$ M melatonin. The reaction was stopped by rapid filtration through GF/B unilters (Whatmann, Maidstone, Kent, UK), followed by three successive washes with ice-cold binding buffer. Data were analyzed with PRISM software (GraphPad Software Inc., San Diego, CA). For saturation assays, the density of binding sites (B<sub>max</sub>) and the dissociation constant of the radioligand (K<sub>D</sub>) values were calculated using Scatchard plot analysis. For displacement experiments, inhibition constants (K<sub>i</sub>) were calculated according to the Cheng–Prusoff equation:  $K_i = IC_{50}/[1 + (L/K_D)]$ , where IC<sub>50</sub> is the inhibitory concentration 50% and *L* is the concentration of 2-[<sup>125</sup>I]iodomelatonin. For the correlation analysis of pK<sub>i</sub> values, the Pearson product–moment correlation coefficient was used.

**X-ray Data.** Suitable crystals of the title compounds were obtained by slow evaporation from **7** at room temperature, and they were mounted on a glass fiber. Diffraction data were collected on an Enraf-Nonius-CAD4 diffractometer with Mo K $\alpha$  radiation ( $\lambda = 0.71073$  Å) at room temperature. Data were measured using  $\theta/2\theta$  scan. The data treatment, polarization, decay corrections, and Gaussian numerical absorption correction were carried out with the JANA98 program.<sup>46</sup> The crystal structure was solved by direct methods using SHELX-97 package.<sup>47</sup> All nonH-atoms were refined anisotropically. The positions of H-atoms were determined via difference Fourier maps and refined with isotropic atomic displacement parameters, with exception of H-atoms of C2, C3, and C4 (Figure 2) that were calculated and fixed on the C-atoms in the ideal geometry. The temperature factors of fixed H-atoms were refined isotropically. One title compound is present in the asymmetric unit. CCDC reference number 151632.

## MOLECULAR MODELING

**Molecular Docking Studies.** The molecular docking studies were performed using Maestro, version 8.5, and SP Glide, version 5.0.<sup>30</sup> The ligand **7** was docked flexibly to the binding site of 1CJW.<sup>31</sup> The coordinates for 1CJW were downloaded from the RCSB Protein Data Bank.<sup>48</sup> In this structure, AANAT is complexed with a bisubstrate analog. The protein was prepared for subsequent grid generation and for docking using the protein preparation wizard tool supplied with Glide. Using this tool, all H-atoms were added, the protonation states for histidine residues were optimized, crystallographic waters not deemed to be important for ligand binding were deleted, and the entire protein was minimized. The structural water near Glu161 was preserved; it was reoriented and adjusted using the commands within the protein preparation wizard tool available within Glide, so that H-bonding between the ligand and the protein could be established. Next, a grid was prepared using the receptor grid generation tool in Glide. With the bisubstrate analog in place, the centroid of the workspace ligand was chosen to define the grid box. The option to dock ligands similar in size to the workspace ligand was selected for determining the grid sizing. For the single-ligand docking, the standard precision mode was selected. The default settings for scaling the van der Waals radii were selected: a scaling factor of 0.8 and a partial charge cutoff of 0.25. H-bond constraints were defined for the docking runs. Indeed, the H-bond between the ligand and the water molecule 1061 or the main chain amide of Leu124 was required. In pose prediction and enrichment studies, a maximum of 20 poses per ligand were saved.

**CoMFA Studies.** The 3D structures of all compounds in the training set were obtained using the Sybyl program package.<sup>49</sup> Their geometries were optimized using the Tripos force field<sup>50</sup> with the distance-dependent dielectric function and the Powell conjugate gradient algorithm<sup>51</sup> (convergence criterion of 0.05 kcal/mol Å). The alignment of the compounds is a crucial step in CoMFA approach. For this study, each molecule was initially aligned on the X-ray crystallographic structure of **7** (Figure 2). The fitting process was performed using an “in-house” developed script written in SPL (Sybyl programming language). This SPL program achieved the fit of all compounds on the template according to selected pairs of atoms. The fixed atoms correspond to the entire molecule **7** excepting atoms C15–C19 (Figure 2). For the CoMFA studies, a 3D cubic lattice box with a grid spacing of 2 and 1 Å was automatically defined around the aligned molecules. The molecular fields—steric and electrostatic—were sampled at each point of the grid using a C sp<sup>3</sup> atom with a +1 charge as probe. The default cutoff ( $E_{\text{cut}} = 30$  kcal/mol) was applied to both fields by considering the “smooth” method. For all field values greater than 1.2  $E_{\text{cut}}$ , a value of  $E_{\text{cut}}$  is applied, and for field values between 0.8 and 1.2  $E_{\text{cut}}$ , the following interpolation is applied

$$E_{\text{smooth}} = \frac{E^2 - 2E_{\text{up}}E + E_{\text{lo}}^2}{2(E_{\text{lo}} - E_{\text{up}})}$$

where *E* is the original field value and  $E_{\text{lo}}$  and  $E_{\text{up}} = 0.8$  and 1.2  $E_{\text{cut}}$ , respectively.

For the cutoff, another method called “abrupt” was also tested, instead of the “smooth” approach. This method simply

sets all probe values that experience interaction energy greater than  $E_{\text{cut}}$  to  $E_{\text{cut}}$ . In this study, the Lennard-Jones parameters and the van der Waals radii were taken from the Tripos force field, and the partial charges were calculated with the semiempirical MOPAC package using the Mulliken method (PM3 Hamiltonian). The method of partial least squares (PLS) implemented in Sybyl was used to construct and validate the models. To determine the optimal number of components, the SAMPLS algorithm was used.<sup>52</sup> The optimum number of components (ONC) was retained for final PLS analyses (first minimum in the standard error).<sup>53</sup> Cross-validation was performed using the leave-one-out procedure, wherein one compound is removed from the data set, and its activity is predicted using the model derived from the rest of the data set. A column filtering of 2.0 kcal/mol was used to reduce noise. Finally, nonvalidated models were produced, and conventional correlation coefficient  $r^2$  and standard error of estimate  $SE_E$  (or  $s$ ) were computed. An alternative to the standard method was also considered to calculate the CoMFA fields. The “box” option was used, which consists of replacing the probe atom by eight probe atoms (making the corners of a cube) centered on the coordinates of the original one. The interactions between each probe atom and target molecule are calculated, and the average value is assigned to the original probe coordinates. With this “box” option, the cutoff is applied by considering the “abrupt” method. From fully validated CoMFA models, contour maps are presented displaying the most relevant regions of the space, where the variations in statistical steric and electrostatic fields are the largest. These contour maps highlight the areas where changes in the molecular field values are strongly associated with changes in binding affinities.

#### ACKNOWLEDGMENT

This work received financial support from the Laboratoires Servier. We thank the Centre de Ressources Informatiques de Haute Normandie (CRIHAN) and the European Community (FEDER) for the molecular modeling software.

#### REFERENCES AND NOTES

- (1) Arendt, J. *Melatonin and the Mammalian Pineal Gland*, Chapman and Hall: London, 1995.
- (2) Korf, H. W.; Schomerus, C.; Stehle, J. H. The Pineal Organ, its Hormone Melatonin, and the Photoneuroendocrine System. *Adv. Anat., Embryol. Cell. Biol.* **1998**, *146*, 1–100.
- (3) Iuvone, P. M.; Tosini, G.; Pozdeyev, N.; Haque, R.; Klein, D. C.; Chaurasia, S. S. Circadian Clocks, Clock Networks, Arylalkylamine N-Acetyltransferase, and Melatonin in the Retina. *Prog. Ret. Eye Res.* **2005**, *24*, 433–456.
- (4) Djeridane, Y.; Toutitout, Y. Melatonin Synthesis in the Rat Harderian Gland: Age- and Time-Related Effects. *Exp. Eye Res.* **2001**, *72*, 487–492.
- (5) Bubenik, G. A. Gastrointestinal Melatonin: Localization, Function, and Clinical Relevance. *Dig. Dis. Sci.* **2002**, *47*, 2336–2348.
- (6) Conti, A.; Conconi, S.; Hertens, E.; Skwarlo-Sonta, K.; Markowska, M.; Maestroni, M. Evidence for Melatonin Synthesis in Mouse and Human Bone Marrow Cells. *J. Pineal Res.* **2000**, *28*, 193–202.
- (7) Slominski, A.; Tobin, D. J.; Zmijewski, M. A.; Wortsman, J.; Paus, R. Melatonin in the Skin: Synthesis, Metabolism and Functions. *Trends Endocrinol. Metab.* **2007**, *19*, 17–24.
- (8) Klein, D. C.; Auerbach, D. A.; Nambodiri, M. A. A.; Wheler, G. H. T. Indole Metabolism in the Mammalian Pineal Gland. In *The pineal Gland V* I, Reiter, R. J., Ed.; CRC Press: Boca Raton, FL, 1981; pp199–227.
- (9) Klein, D. C.; Baler, R.; Roseboom, P. H.; Weller, J. L.; Bernard, M.; Gastel, J. A.; Zatz, M.; Iuvone, P. M.; Cahill, G. M.; Falcón, J.; Cahill, G.; Cassone, V. M.; Coon, S. L. The Molecular Basis of the Pineal Melatonin Rhythm: Regulation of Serotonin N-acetylation. In *Handbook of Behavioral State control: Cellular and Molecular Mechanisms*, Lydic, R., Baghdoyan, H. A., Ed.; CRC Press: Boca Raton, FL, 1999; pp45–59.
- (10) Axelrod, J. The Pineal Gland: a Neurochemical Transducer. *Science* **1974**, *184*, 1341–1348.
- (11) Reiter, R. J. Pineal Melatonin: Cell Biology of its Synthesis and of its Physiological Interactions. *Endocr. Rev.* **1991**, *12*, 151–180.
- (12) Klein, D. C.; Coon, S. L.; Roseboom, P. H.; Weller, J. L.; Bernard, M.; Gastel, J. A.; Zatz, M.; Iuvone, P. M.; Rodriguez, I. R.; Begay, V.; Falcon, J.; Cahill, G. M.; Cassone, V. M.; Baler, R. The Melatonin Rhythm-Generating Enzyme: Molecular Regulation of Serotonin N-Acetyltransferase in the Pineal Gland. *Recent Prog. Horm. Res.* **1997**, *52*, 307–357.
- (13) Mody, S. M.; Hu, Y.; Ho, M. K. C.; Wong, Y. H. In Search of Novel and Therapeutically Significant Melatonergic Ligands. *Recent Pat. CNS Drug Discov.* **2007**, *2*, 241–245.
- (14) Zlotos, D. P. Recent Advances in Melatonin Receptor Ligands. *Arch. Pharm. (Weinheim, Ger.)* **2005**, *338*, 229–247.
- (15) Pierpaoli, W.; Regelson, W.; Colman, C. *The Melatonin Miracle. Nature's Age-Reversing, Disease-Fighting, Sex-Enhancing Hormone*, Pocket Books: New York, 1995.
- (16) Reppert, S. M.; Weaver, D. R. Melatonin Madness. *Cell* **1995**, *83*, 1059–1062.
- (17) Lewy, A. J.; Sack, R. L.; Miller, L. S.; Hoban, T. M. Antidepressant and Circadian Phase-Shifting Effects of Light. *Science* **1987**, *235*, 352–354.
- (18) Bonhomme, N.; Esposito, E. Involvement of Serotonin and Dopamine in the Mechanism of Action of Novel Antidepressant Drugs: a Review. *J. Clin. Psychopharmacol.* **1998**, *18*, 447–454.
- (19) Zheng, W.; Cole, P. A. Serotonin N-Acetyltransferase: Mechanism and Inhibition. *Curr. Med. Chem.* **2002**, *9*, 1187–1199.
- (20) Shen, S.; Bremont, B.; Serraz, I.; Andrieux, J.; Poncet, A.; Mathe-Allainmat, M.; Chanut, E.; Trouvin, J. H.; Langlois, M. Structure-Activity Relationships for Substrates and Inhibitors of Pineal 5-Hydroxytryptamine-N-Acetyltransferase: Preliminary Studies. *Eur. J. Pharmacol.* **1996**, *307*, 133–140.
- (21) Ferry, G.; Loynel, A.; Kucharczyk, N.; Bertin, S.; Rodriguez, M.; Delagrangé, P.; Galizzi, J. P.; Jacoby, E.; Volland, J. P.; Lesieur, D.; Renard, P.; Canet, E.; Fauchère, J. L.; Boutin, J. A. Substrate Specificity and Inhibition Studies of Human Serotonin N-Acetyltransferase. *J. Biol. Chem.* **2000**, *275*, 8794–8805.
- (22) Page, A. I. Enzyme Inhibition. In *Comprehensive Medicinal Chemistry*, volume 2; Sammes, P. G., Ed.; Pergamon Press: New York, 1990; pp. 61–87.
- (23) Khalil, E. M.; Cole, P. A. A Potent Inhibitor of the Melatonin Rhythm Enzyme. *J. Am. Chem. Soc.* **1998**, *120*, 6195–6196.
- (24) Khalil, E. M.; De Angelis, J.; Ishii, M.; Cole, P. A. Mechanism-Based Inhibition of the Melatonin Rhythm Enzyme: Pharmacologic Exploitation of Active Site Functional Plasticity. *Proc. Natl. Acad. Sci. U.S.A.* **1999**, *96*, 12418–12423.
- (25) Kim, C. M.; Cole, P. A. Bisubstrate Ketone Analogues as Serotonin N-Acetyltransferase Inhibitors. *J. Med. Chem.* **2001**, *44*, 2479–2485.
- (26) Zheng, W.; Scheibner, K. A.; Ho, A. K.; Cole, P. A. Mechanistic Studies on the Alkyltransferase Activity of Serotonin N-Acetyltransferase. *Chem. Biol.* **2001**, *8*, 379–389.
- (27) Ferry, G.; Ubeaud, C.; Mozo, J.; Pean, C.; Hennig, P.; Rodriguez, M.; Scoul, C.; Bonnaud, A.; Nosjean, O.; Galizzi, J. P.; Delagrangé, P.; Renard, P.; Volland, J. P.; Yous, S.; Lesieur, D.; Boutin, J. A. New Substrate Analogues of Human Serotonin N-Acetyltransferase Produce in Situ Specific and Potent Inhibitors. *Eur. J. Biochem.* **2004**, *271*, 418–428.
- (28) Beaurain, N.; Mesangeau, C.; Chavatte, P.; Ferry, G.; Audinot, V.; Boutin, J. A.; Delagrangé, P.; Bennejean, C.; Yous, S. Design, Synthesis and in Vitro Evaluation of Novel Derivatives as Serotonin N-Acetyltransferase Inhibitors. *J. Enzyme Inhib. Med. Chem.* **2002**, *17*, 409–414.
- (29) Szewczuk, L. M.; Saldanha, S. A.; Ganguly, S.; Bowers, E. M.; Javoroncov, M.; Karanam, B.; Culhane, J. C.; Holbert, M. A.; Klein, D. C.; Abagyan, R.; Cole, P. A. De Novo Discovery of Serotonin N-Acetyltransferase Inhibitors. *J. Med. Chem.* **2007**, *50*, 5330–5338.
- (30) Friesner, R. A.; Banks, J. L.; Murphy, R. B.; Halgren, T. A.; Klicic, J. J.; Mainz, D. T.; Repasky, M. P.; Knoll, E. H.; Shaw, D. E.; Shelley, M.; Perry, J. K.; Francis, P.; Shenkin, P. S. Glide: A New Approach for Rapid, Accurate Docking and Scoring. 1. Method and Assessment of Docking Accuracy. *J. Med. Chem.* **2004**, *47*, 1739–1749.
- (31) Hickman, A. B.; Nambodiri, M. A.; Klein, D. C.; Dyda, F. The Structural Basis of Ordered Substrate Binding by Serotonin N-Acetyltransferase: Enzyme Complex at 1.8 Å Resolution with a Bisubstrate Analog. *Cell* **1999**, *97*, 361–369.
- (32) (a) Cramer, R. D., III; Patterson, D. E.; Bunce, J. D. Comparative Molecular Field Analysis (CoMFA). 1. Effect of Shape on Binding of Steroids to Carrier Proteins. *J. Am. Chem. Soc.* **1988**, *110*, 5959–5967. (b) Cramer, R. D., III; DePriest, S. A.; Patterson, D. E.; Hecht, P. The Developing Practice of Comparative Molecular Field Analysis.

- In 3D QSAR in Drug Design: Recent Advances, Kubinyi, H., Ed.; ESCOM: Leiden, The Netherlands 1993; pp443–485. (c) Cramer, R. D., III; Patterson, D. E.; Bunce, J. D. Recent Advances in Comparative Molecular Field Analysis (CoMFA). *Prog. Clin. Biol. Res.* **1989**, 291, 161–165.
- (33) Allen, F. H. The Cambridge Structural Database: a Quarter of a Million Crystal Structures and Rising. *Acta Crystallogr.* **2002**, B58, 380–388.
- (34) Clark, M.; Cramer III, R. D. The Probability of Chance Correlation Using Partial Least Square (PLS). *Quant. Struct.-Act. Relat.* **1993**, 12, 137–145.
- (35) Melville, J. L.; Hirst, J. D. On the Stability of CoMFA Models. *J. Chem. Inf. Comput. Sci.* **2004**, 44, 1294–1300.
- (36) Klebe, G.; Abraham, U.; Mietzner, T. Molecular Similarity Indices in a Comparative Analysis (CoMSIA) of Drug Molecules to Correlate and Predict their Biological Activity. *J. Med. Chem.* **1994**, 37, 4130–4146.
- (37) Albers, W. M.; Canters, G. W.; Reedijk, J. Preparation of Extended Di(4-pyridyl)thiophene Oligomers. *Tetrahedron* **1995**, 51, 3895–3904.
- (38) Wu, R.; Schumm, J. S.; Pearson, D. L.; Tour, J. M. Convergent Synthetic Routes to Orthogonally Fused Conjugated Oligomers Directed toward Molecular Scale Electronic Device Applications. *J. Org. Chem.* **1996**, 61, 6906–6921.
- (39) Vallgarda, J.; Appelberg, U.; Arvidsson, L.-E.; Hjorth, S.; Svensson, B. E.; Hacksell, U. Trans-2-Aryl-N,N-dipropylcyclopropylamines: Synthesis and Interactions with 5-HT<sub>1A</sub> Receptors. *J. Med. Chem.* **1996**, 39, 1485–1493.
- (40) Van den Hoven, B. G.; Alper, H. The First Regioselective Hydroformylation of Acetylenic Thiophenes Catalyzed by a Zwitterionic Rhodium Complex and Triphenyl Phosphite. *J. Org. Chem.* **1999**, 64, 9640–9645.
- (41) Zheng, A.; Wang, W.; Zhang, H.; Wang, B. Two New Improved Approaches to the Synthesis of Coumarin-Based Prodrugs. *Tetrahedron* **1999**, 14, 4237–4254.
- (42) Ferry, G.; Mozo, J.; Ubeaud, C.; Berger, S.; Bertrand, M.; Try, A.; Beauverger, P.; Mesangeau, C.; Delagrangé, P.; Boutin, J. A. Characterization and Regulation of a CHO Cell Line Stably Expressing Human Serotonin N-Acetyltransferase (EC 2.3.1.87). *Cell. Mol. Life Sci.* **2002**, 59, 1395–1405.
- (43) Ferry, G.; Loynel, A.; Kucharczyk, N.; Bertin, S.; Rodriguez, M.; Delagrangé, P.; Galizzi, J. P.; Jacoby, E.; Volland, J. P.; Lesieur, D.; Renard, P.; Canet, E.; Fauchere, J. L.; Boutin, J. A. Substrate Specificity and Inhibition Studies of Human Serotonin N-Acetyltransferase. *J. Biol. Chem.* **2000**, 275, 8794–8805.
- (44) Bradford, M. M. A Rapid and Sensitive Method for the Quantitation of Microgram Quantities of Protein Utilizing the Principle of Protein-dye Binding. *Anal. Biochem.* **1976**, 72, 248–254.
- (45) Audinot, V.; Mailliet, F.; Lahaye-Brasseur, C.; Bonnaud, A.; Le Gall, A.; Amossé, C.; Dromaint, S.; Rodriguez, M.; Nagel, N.; Galizzi, J. P.; Malpoux, B.; Guillaumet, G.; Lesieur, D.; Lefoulon, F.; Renard, P.; Delagrangé, P.; Boutin, J. A. New Selective Ligands of Human Cloned Melatonin MT1 and MT2 Receptors. *Naunyn-Schmiedeberg's Arch. Pharmacol.* **2003**, 367, 553–561.
- (46) Petricek, V.; Dusek, M. JANA98; *The Crystallographic Computing System*; Institute of Physics: Praha, Czech Republic, 1998.
- (47) (a) Sheldrick, G. M. Phase Annealing in SHELX-90: Direct Methods for Larger Structures. *Acta Crystallogr.* **1990**, A46, 467–473. (b) Sheldrick, G. M. SHELX-97; *Program for the Refinement of Crystal Structures*; University of Göttingen: Göttingen, Germany, 1997.
- (48) Berman, H. M.; Westbrook, J.; Feng, Z.; Gilliland, G.; Bhat, T. N.; Weissig, H.; Shindyalov, I. N.; Bourne, P. E. The Protein Data Bank. *Nucleic Acids Res.* **2000**, 28, 235–242.
- (49) Sybyl 6.9; Tripos Inc.: St Louis, MO, 2003.
- (50) Clark, M.; Cramer, R. D., III; van Opdenbosch, N. Validation of the General-Purpose Tripos 5.2 Force-Field. *J. Comput. Chem.* **1989**, 10, 982–1012.
- (51) Powell, M. J. D. Restart Procedures for the Conjugate Gradient Method. *Math. Program.* **1977**, 12, 241–254.
- (52) Bush, B. L.; Nachbar, R. B., Jr. Sample-Distance Partial Least Squares: PLS Optimized for Many Variables, with Application to CoMFA. *J. Comput.-Aided Mol. Des.* **1993**, 7, 587–619.
- (53) Kubinyi, H.; Abraham, U. Practical Problems in PLS Analyses. In *3D-QSAR in Drug Design-Theory, Methods and Applications*, Kubinyi, H., Ed.; ESCOM Science Pub: Leiden, The Netherlands 1993; pp717–728.

CI9004805